Nat Chem Biol. Author manuscript; available in PMC 2017 April 10.

Published in final edited form as:
Nat Chem Biol. 2016 December ; 12(12): 1046–1052. doi:10.1038/nchembio.2192.

Competing charge transfer pathways at the photosystem II-electrode interface

Jenny Z. Zhang[1], **Katarzyna P. Sokol**[1], **Nicholas Paul**[1], **Elisabet Romero**[2], **Rienk van Grondelle**[2], and **Erwin Reisner**[1,*]

[(1)]Department of Chemistry, University of Cambridge, Lensfield Road, Cambridge CB21EW, UK
[(2)]Department of Physics and Astronomy, VU University, De Boelelaan 1081, NL-1081 HV Amsterdam, The Netherlands

Abstract

The integration of the water-oxidation enzyme, photosystem II (PSII), into electrodes allows the electrons extracted from water-oxidation to be harnessed for enzyme characterization and driving novel endergonic reactions. However, PSII continues to underperform in integrated photoelectrochemical systems despite extensive optimization efforts. Here, we performed protein-film photoelectrochemistry on spinach and *Thermosynechococcus elongatus* PSII, and identified a competing charge transfer pathway at the enzyme-electrode interface that short-circuits the known water-oxidation pathway: photo-induced O_2 reduction occurring at the chlorophyll pigments. This undesirable pathway is promoted by the embedment of PSII in an electron-conducting matrix, a common strategy of enzyme immobilization. Anaerobicity helps to recover the PSII photoresponses, and unmasked the onset potentials relating to the Q_A/Q_B charge transfer process. These findings have imparted a fuller understanding of the charge transfer pathways within PSII and at photosystem-electrode interfaces, which will lead to more rational design of pigment-containing photoelectrodes in general.

Photosystem II (PSII) is a 700 kDa dimeric pigment-protein complex that resides in the membranes of oxygen evolving photosynthetic organisms.1 It is unique in nature in its ability to photocatalyze water-oxidation to liberate H^+, O_2 and electrons, which is the first step of oxygenic photosynthesis. The study of PSII functionality is important in both fundamental and applied sciences,2 in particular for providing lessons for solar fuel technologies where water-oxidation is a bottleneck.3

*Corresponding author: reisner@ch.cam.ac.uk; web: http://www-reisner.ch.cam.ac.uk/.

Author Contributions

J.Z.Z. and E.Reisner conceived the research, J.Z.Z. performed all experiments and wrote the manuscript. K.P. provided the ITO electrodes. E.Romero and R.v.G provided the spinach PSII. J.Z.Z, N.P., E.Romero and E.Reisner added to the discussion and contributed to the preparation of the manuscript. E.Reisner supervised this work.

Competing financial interests

The authors declare no competing financial interests.

Europe PMC Funders Author Manuscripts

Protein-film photoelectrochemistry (PF-PEC) is a direct and sensitive method of characterizing light-induced redox events arising from photoactive proteins on an electrode surface.4,5 Recent advancements in electrode design6,7 has enabled PF-PEC to become a platform in which photosystems could be characterized,4 used in photocatalyst benchmarking,8 and used to drive novel endergonic reactions.6,9 For example, PSII was recently coupled to a hydrogenase photoelectrochemically to drive light-driven water-splitting via an unnatural photobiological pathway.6 The study followed the development of a hierarchically structured inverse opal mesoporous indium tin oxide (ITO) electrode that enabled exceptionally high loadings of PSII and the subsequent quantification of O_2 evolution.

The mechanism by which PSII performs water-oxidation photocatalysis is shown in Figure 1A. Light energy is harvested mainly at the chlorophyll (Chl) *a* pigments in the CP43 and CP47 antenna subunits, and funneled to the reaction center (RC) complex. Due to the energetic disorder, ultrafast charge generation in the RC proceeds via two pathways depending on protein configuration,10,11 and quantum coherence promotes the high efficiency of the initial charge separation events.12 The photogenerated electrons are passed via a pheophytin to an immobile plastoquinone, Q_A, then to a mobile plastoquinone, Q_B.13 Upon two electron reductions, the Q_B diffuses out of its pocket and shuttles the electrons to a cytochrome b_6f within the thylakoid membrane. Concurrently, the photogenerated holes at the RC complex move in the opposite direction via a tyrosine to enter the Kok cycle, the catalytic cycle for water-oxidation.

The slow step in PSII charge transfer is the diffusional step between PSII's terminal electron acceptor Q_B and the subsequent electron acceptor.4 However, when a high concentration of electron mediators is present or the PSII is efficiently wired to an electrode to allow direct interfacial electron transfer (ET), turn-over-frequency values of up to 250 mol O_2 (mol PSII)$^{-1}$ s^{-1} can in principle be achieved, calculated based on the slowest step in the Kok cycle.14 Despite extensive efforts to optimize the ET efficiency between PSII and the electrode, the turn-over-frequency values reported for immobilized PSII on electrodes typically fall below 15 s^{-1}.4,6 The low ET efficiency exhibited by PSII at the electrode interface is currently poorly understood.

Due to the large dimension of PSII (11 nm × 10 nm × 20 nm per dimer) and the spatial arrangements of the cofactors within the enzyme (Supplementary Results, Supplementary Figure 1), PSII must be interfaced with the electrode via its stromal side to enable efficient electronic communication between the Q_A/Q_B and the electrode. Some progress has been made in controlling PSII orientation on electrodes using surface linkers endowed with charged functionalities and Histags.15,16 Additionally, PSII is commonly embedded in electron-accepting matrices or layer-by-layer structures comprising of redox-active polymers or carbon-based sp^2 hybridized materials,17,18 which allows multiple layers of PSII to be electronically connected to the electrode regardless of orientation. Thus far, all efforts to more efficiently wire PSII to the electrode have not resulted in the step change in performance desired.

Here, we identified a new light-induced charge transfer pathway at the PSII-electrode interface that competes against the known water-oxidation pathway (Figure 1B). We reveal that the competing pathway arises from antenna Chl *a* pigments participating in the photo-induced reduction of O_2 near the electrode. This pathway could be attenuated/amplified by the O_2 concentration, and the presence of an electron-accepting matrix. Anaerobicity enhances the photoresponse of PSII and unmasks the true onset potential of the photoanodic currents, allowing for the Q_A/Q_B charge transfer step to be studied using PF-PEC.

Results

This study used PSII core complexes derived from two different sources: the higher plant spinach, and the cyanobacterium *Thermosynechococcus elongatus* (*T. elongatus*). Inverse opal mesoporous ITO electrodes (Supplementary Figure 2) were employed for to their ability to accommodate high and stable enzyme loadings.6

Photoelectrochemical water-oxidation with PSII

We first characterized the photoresponse of spinach and *T. elongatus* PSII by performing stepped chronoamperometry scans under chopped light illumination on the two PSII adsorbed on ITO electrodes (Figure 2). The photoresponses have been normalized to reflect the photocurrent observed per mg Chl *a* deposited on the electrode. Both PSII gave rise to photoanodic currents at applied potentials above 0.2 V vs SHE, which have previously been assigned to water-oxidation.7,8 Unassigned photocathodic currents can be observed below 0.2 V vs SHE (see next section). Bare (protein-free) ITO electrodes did not give rise to photocurrents under the same conditions (Supplementary Figure 3).

The photoanodic response can be explained by the energy/charge transfer mechanisms depicted in Figure 1B. When the Fermi level of the electrode (controlled by the applied potential) is more positive than the redox potentials of the Q_A/Q_B within PSII, PSII in the correct orientation can transfer electrons directly to the electrode when illuminated to result in a rise in anodic current.

Photo-induced Chl a charge transfer in PSII

Previous PF-PEC studies have typically measured photocurrents densities at applied potentials of > 0.4 vs SHE to determine PSII performance.4 As such, the photocathodic currents observed below 0.2 V *vs* SHE (Figure 2) have not been reported and are unassigned. The origin of the photocathodic current is unlikely to involve the hole-transfer cofactors present in the water-oxidation pathway since the tyrosine and Mn_4Ca cluster are both buried 3 nm deep within the protein shell.1 The photocathodic response is more likely to stem from interactions between the electrode and photo-responsive co-factors that reside near the surface of the protein shell such as the many Chl *a* and β-carotene (β-car) pigments located in the antenna subunits (each antenna subunit has around 15 Chl *a* pigments, most of which are within 20 Å from the protein shell in the transmembrane region of the enzyme, 7,19,20 see Supplementary Figure 1). This is made more likely by the mesoporous substructure of the electrode, which can contact multiple sides of individual enzymes.

To identify the source of the photocathodic currents, we performed stepped chronoamperometry scans with chopped illumination on isolated antenna CP43 and RC complex subunits (Figure 1), as well as on Chl *a* and β-car molecules. The isolated RC complex used in this study has lost the plastoquinones, non-heme Fe and the Mn_4Ca cluster in the isolation process.

We observed clear photocathodic currents for the adsorbed antenna CP43, RC complex, and the isolated Chl *a* molecules (onset potential ~0.5 V vs SHE, Figure 2), but not for the β-car molecules. The observation that all Chl *a*-containing components generated photocathodic currents indicates that photo-induced ET can occur from the ITO to free Chl *a* molecules, as well as to Chl *a* within the protein shell. The adsorbed RC complex gave rise to larger photocathodic currents than the adsorbed PSII core complexes and the antenna subunit, which may be attributed to the charge transfer-active Chl *a* pigments within the exposed RC complex forming electronic contact with the electrode surface. It also cannot be excluded that other exposed cofactors, such as the Tyr^+ can participate in charge transfer. The antenna CP43 subunit gave rise to a relatively smaller normalized photocathodic response despite having the highest density of embedded Chl *a* pigments. This may be attributed to less favorable protein-electrode interactions due to the presence of the hydrophobic transmembrane domain.

To better understand the nature of the photocurrents, we obtained the action spectra (photoresponse at different wavelengths) of the PSII core complexes and isolated Chl *a* pigments on ITO electrodes at wavelengths 720 to 460 nm at applied potentials of 0 and 0.5 V vs SHE (Supplementary Figure 4). At 0.5 V vs SHE, bare ITO exhibited photoanodic response at wavelengths < 540 nm, and adsorbed Chl *a* molecules exhibited no photoresponse (taking into account the ITO background). Photoanodic responses (maximum at ~680 nm) were observed for both PSII, which corroborates with their respective absorption profile (Supplementary Figure 4A). At 0 V vs SHE, bare ITO exhibited no photoresponse, and adsorbed Chl *a* exhibited photocathodic responses (maximum at 660-680 nm) consistent with its absorption spectrum. Photocathodic responses (maximum ~680 nm) were observed for both PSII core complexes, which is slightly red-shifted compared to free Chl *a* and consistent with their absorption profile (Supplementary Figure 4B). This is further evidence that the photocathodic response stems from the PSII core complexes, with large involvement from the Chl *a* pigments.

The photoresponse of Chl *a* films on semiconductors has been studied in the past.21,22 Photoexcited states (Chl *a**) were shown to transfer electrons to the conduction band of the semiconductor to give rise to photoanodic currents, followed by the regeneration of oxidized Chl *a* by a chemical electron donor.23,24 However, in the absence of the electron donor and in the presence of O_2 under a relatively negative applied potential, Chl *a** has been observed to produce a photocathodic current,23 which corroborates with our findings. The authors proposed that the ET from the Chl *a** to the O_2 is the primary step in the mechanism, followed by hole migration from the electrode to the Chl a^+ (Chl a^+, E_m: ~0.78 V vs SHE)25. The alternative mechanism is that hole migration from the photoexcited Chl *a** to the electrode (at applied potential < ~0.78 V vs SHE) is the primary step, followed by the reduction of dissolved O_2 (E_m ($O_2/O_2^{\bullet-}$): ~ –0.33 V vs SHE)26 by the Chl a^- (E_m: ~ –1.1 V

vs SHE)25,27. A recent study has reported that organic dyes adsorbed on ITO electrodes can exhibit analogous photocathodic behavior in the presence of suitable electron acceptors such as I_3^- under a relatively negative applied potential.28 The authors used transient absorption spectroscopy to show that the primary step is the photo-injection of the hole from the photoexcited dye into the conduction band of the ITO electrode, which supports the second proposed mechanism where Chl a^- is generated.

Photoelectrochemical O_2 reduction by PSII

In water-splitting systems, the presence of O_2 is unavoidable since it is liberated in the process of water-oxidation. Although photoexcited Chl *a* triplet states (^{3}Chl *a*) within PSII are known to undergo energy transfer processes with O_2 (via ^{3}Chl *a*-$^3O_2$ annihilation)29 to generate $^1O_2$, charge transfer between Chl *a* and O_2 have not been reported. To clarify the role of O_2 as an electron acceptor in the observed photocathodic process, we repeated stepped chronoamperometry scans of adsorbed PSII core complexes and Chl *a* molecules in the presence and absence of atmospheric O_2 (Figure 3). In anaerobic conditions, the photocathodic pathway was diminished in all cases, confirming the role of O_2 as an electron acceptor in the proposed pathway (Figure 1B). Anaerobicity increased the photoanodic currents arising from the PSII core complexes most significantly at applied potentials of ≤ 0.3 V vs SHE since the onset potential of the competing photocathodic current is around 0.3 V vs SHE.

To elucidate the rate-limiting step in the photocathodic current generation, we repeated the experiment in electrolyte solutions purged with different concentrations of O_2 gas (Supplementary Figure 5). We observed the photocathodic currents increased with the concentration of O_2 introduced into the system, which is consistent with the ET from the Chl *a* to the O_2 being the rate-limiting step. This is not surprising as the reduction of O_2 by Chl a* is diffusion rate-limited, unlike the charge transfer between the electrode surface and the photoexcited pigment.

Due to the low concentrations of reduced O_2 species expected to be produced, we employed electrochemical techniques to detect any products from O_2 reduction present on the electrode surface following irradiation. We performed cyclic voltammetry (CV) scans on adsorbed Chl *a* under aerobic conditions (Supplementary Figure 6A) and observed currents from O_2 reduction at potentials below 0 V vs SHE in the absence of light. Following prolonged red-light illumination (> 5 min), we observed a new cathodic wave with an onset of ~0.2 V vs SHE. This was not present in the second or subsequent scans, nor in anaerobic conditions (Supplementary Figure 6B). The cathodic wave with an onset of ~0.2 V vs SHE did not appear when we repeated the experiment under aerobic conditions with catalase present in the electrolyte solution. To determine whether the photogeneration of the cathodic wave was due to H_2O_2 reduction, we performed a CV scan of a 0.14 mM H_2O_2 solution using a bare ITO electrode (Supplementary Figure 6C) under anaerobic conditions. We chose this concentration of H_2O_2 to correspond to half the concentration of dissolved O_2 in an aqueous solution since any H_2O_2 formed would be from the dissolved O_2. We observed a cathodic wave with an onset potential of 0.2 V vs SHE, which disappears with the addition of catalase. We therefore assign this wave to H_2O_2 reduction. This result affirms the activity

of the catalase, and supports the photo-reduction of O_2 by the Chl *a* to yield H_2O_2, most likely via the formation of $O_2^{\bullet-}$ followed by disproportionation to H_2O_2.30

To clarify whether the photo-generated reactive oxygen species (ROS) on the electrode surface serve as electron acceptors and contribute to the photocathodic pathway, we investigated the effects of stirring (to induce changes to the concentration gradient of diffusional species at the electrode surface) on the photocathodic response. We observed no differences in the photocathodic response upon the commencement of stirring during a chronoamperometry scan of adsorbed Chl *a* at 0.1 V vs SHE (Supplementary Figure 7). The addition of SOD and catalase also had no effect on the photocurrent density, indicating that $O_2^{\bullet-}$ and H_2O_2 do not serve as electron acceptors in the photocathodic pathway.

The embedment of PSII in a fullerene matrix

In addition to O_2 acting as an electron acceptor for photoexcited Chl *a* pigments, the use of electron accepting matrices to improve the PSII-electrode interface may also facilitate undesirable charge escape pathways. To test this hypothesis, we performed PF-PEC on Chl *a* and PSII co-adsorbed with an excess of the semi-water soluble fullerene C_{60}-(N,N-dimethyl pyrrolidinium) iodide (C_{60}-DMePyI). The fullerene derivative was chosen for the assembly of the conductive matrix due to its high electron mobility, appropriate dimensions (~1 nm) for facile penetration through the porous electrode structure, relative hydrophilicity for interactions with PSII, and appropriate reduction potentials for the Q_A/Q_B.31

We performed background stepped chronoamperometry scans of C_{60}-DMePyI (45 nmol) adsorbed on ITO and observed photocathodic response under aerobic conditions, but not under anaerobic conditions (Supplementary Figure 8). This indicates that the fullerene can also participate in photo-induced O_2 reduction. Furthermore, the adsorbed C_{60}-DMePyI exhibited photoanodic response both in aerobic and anaerobic conditions, possibly due to the photo-oxidization of buffer components at more positive applied potentials. Regardless, the photoanodic and photocathodic responses were relatively small at the potential window relevant for this study, and will be taken into account in the co-adsorption experiments.

We next performed the same scans on the PSII/Chl *a* in the presence and absence of the C_{60}-DMePyI matrix under aerobic and anaerobic conditions (Figure 3). In the presence of the C_{60}-DMePyI matrix under aerobic conditions, we observed enhanced photoanodic and photocathodic currents in all cases. This indicates that the non-specific interactions between PSII and the electron conducting matrix has led to enhancements of both ET pathways at the PSII-electrode interface (Figure 1B). The photocathodic enhancements were dampened under Ar purged conditions, indicating that C_{60}-DMePyI enhances the O_2 reduction pathways. This may be explained by efficient ET from ^{1}Chl *a** or ^{3}Chl *a** to the fullerene, which has been previously documented for an analogous solution system.32 The C_{60}^- has also been known to transfer electrons to acceptors, including O_2.33 If the reduction of O_2 by the Chl *a* is the slow step in the system (Figure 3D) as proposed, then the C_{60}-DMePyI in the photocathodic current enhancement is facilitating charge transfer from the Chl a^- to open up the bottleneck. Additionally, the fullerene may act as a mediator between the electrode and the Chl *a* pigment to further enhance the photocathodic pathway. As such, the electron conductive matrix may be facilitating the photocathodic pathway via two mechanisms.

The presence of the C_{60}-DMePyI matrix enhanced the photoanodic response from spinach and *T. elongatus* PSII, but not for Chl *a* (taking into account the background photoanodic response of C_{60}-DMePyI shown in Supplementary Figure 8). This is expected since the fullerene is likely to facilitate the ET from the reduced Q_A/Q_B to the ITO electrode. The photoanodic current enhancement was greatest under anaerobic conditions, particularly at applied potentials of 0.3 to 0.5 V vs SHE. Such an enhancement could be attributed to the diminishment of the O_2 reduction pathway, which then leads to the electrons being more efficiently mediated from the Q_A/Q_B to the electrode, and enhanced PSII water-oxidation.

PF-PEC characterization of Q_A and Q_B

The use of PF-PEC in the characterization of the redox properties of Q_A/Q_B has not been reported previously. This may in large part be due to the photocathodic interference reported here, which masks the onset of the photoanodic signals corresponding to the ET events from the plastoquinones to the electrode. Knowledge of the redox properties of the plastoquinones is important since they are the terminal electron acceptors within PSII and serve as the electron gate that 'opens' the RC complex for water-oxidation. Appropriate pairing of synthetic electron acceptors to the redox potential of the plastoquinones is essential for overall PSII water-oxidation performance.

We performed stepped chronoamperometry scans on adsorbed *T. elongatus* and spinach PSII using small potential steps (0.025 V) near the expected redox potentials of the Q_A and Q_B, which has been reported to differ by ~80 mV.34,35 We scanned in both the anodic and cathodic directions, and observed a small difference in the onset potential. Scanning in the anodic direction minimizes the presence of O_2 near the onset potential (defined here as the potential at which the photocurrent becomes a positive non-zero value) and is likely to yield a more reliable value. Figure 4 shows the normalized photoresponses (100% at 0.6 V vs SHE) scanned in the anodic direction, plotted as a function of the applied potential (raw data are shown in Supplementary Figures 9 and 10). The normalized photoresponses scanned in the cathodic direction is shown in Supplementary Figure 11.

In the scans of both PSII, Ar purging produced a significant cathodic shift in the onset potentials due to the elimination of the photocathodic interference. We observed onset potentials of ~75 and 100 mV vs SHE for spinach and *T. elongatus* PSII, respectively. Since Q_B is the natural terminal electron acceptor, the onset potentials are likely to correspond to the Q_B if it is present, with possible flow-over contributions from Q_A.

The Q_B can be displaced by high concentrations of an inhibitor such as 3-(3,4-dichlorophenyl)-1,1-dimethylurea (DCMU), in which case the electrons are believed to transfer directly from Q_A to the electrode,7 allowing Q_A to be more selectively studied. The presence of DCMU shifted the onset potential of spinach PSII by ~100 mV. Assuming that the Q_B is displaced by DCMU, we assigned the onset redox potential for Q_A/Q_A^- in spinach PSII to ~ –25 mV vs SHE. The presence of DCMU did not affect the onset potential of *T. elongatus* PSII, which may be attributed to Q_B being lost before the PF-PEC experiment. As such, we estimate the onset potential of the Q_A in of *T. elongatus* PSII to be ~100 mV vs SHE.

Based on the onset potentials of the photoanodic currents, the trends in E_m values of the plastoquinones can be compared. In the case of spinach PSII, we estimate that the E_m (Q_B/Q_B^-) will be more cathodic than E_m (Q_A/Q_A^-) by 100 mV, which corroborates with the literature.34,35 Similarly, we estimate that the E_m (Q_A/Q_A^-) value of *T. elongatus* PSII is more positive compared to that of spinach PSII by 100 mV, which also corroborates with literature.36 The difference in E_m (Q_A/Q_A^-) values of PSII from different organisms may stem from variations in the protein environment of the Q_A pocket. A better knowledge of the structures of eukaryote PSII will help to clarify this issue in the future.

We cannot estimate the E_m (Q_A/Q_A^-) and E_m (Q_B/Q_B^-) values in a straight-forward manner from this study. Both PSII show a linear current-potential response at higher driving forces (> 0.2 V vs SHE, Fig. 4). This is expected for unmediated and randomly oriented enzymes on an electrode surface where a broad distribution in distance (and rates of interfacial ET) between the buried plastoquinones and the electrode exists.37 However, small shoulders are visible at the lower potentials (< 0.2 vs SHE) that may correspond to redox couples from the plastoquinones (Supplementary Figure 12). It may be possible to resolve these shoulders in the future, for example with better control of enzyme orientation on the electrodes or more advanced electrochemical methods.38

Previous methods of estimating E_m (Q/Q_A^-) values in PSII include the use of chemical titrations34,39 fluorescence-based spectroelectrochemistry,40 and protein film voltammetry; 41 all of which have limitations. Consequently, a consensus of the values has yet to be reached. PF-PEC is a direct means of measuring ET originating from the plastoquinones in open (irradiated) PSII complexes. Based on the onset potentials, the E_m (Q/Q_A^-) values derived from PF-PEC would be significantly more positive than those obtained using traditional methods.34,39 It may be that PF-PEC introduces a positive bias in the estimation of the E_m due to interfacial resistance. It may also be that the O_2 produced by PSII cannot be fully removed by Ar purging alone due to in situ production of O_2. To investigate this possibility, we repeated the scans for adsorbed spinach PSII in the presence of the oxygen scavenger glucose-catalase-glucose oxidase system in addition to performing Ar purging (Supplementary Figure 13). We observed a negative shift of ~25 mV in the onset potential, which indicates that further depletion of O_2 can help to unmask the true PSII onset potential. However, the presence of residue O_2 does not fully explain the relatively positive redox potentials measured by PF-PEC.

Regardless, PF-PEC provides valuable insights into the terminal electron acceptors of the water-oxidation pathway in PSII. For example, soluble redox mediators such as 2,6-dichlorobenzoquinone (DCBQ) are commonly used as a Q_B mimic or to mediate ET from any remaining Q_B to the electrode (Figure 1B).42,43 In the presence of DCBQ, we observed onset potentials for both PSII to be ~250 mV vs SHE (Figure 4). We can derive the E_m ($DCBQ/DCBQ^-$) value of ~310 mV vs SHE from the limiting photocurrents (Supplementary Figure 12), which is consistent with the value of 320 mV vs SHE derived from CV scans performed in the same buffer conditions (Supplementary Figure 14). We learned that although DCBQ can mediate electrons from PSII to the electrode, the E_m value of DCBQ is mismatched with the terminal electron acceptor in PSII by at least 200 mV.

Discussion

This study has provided a fuller picture of the ET pathways at the PSII-electrode interface, and showed how the overall PSII photoresponse is the net result of different competing pathways. Figure 5 is a summary of energy/charge transfer pathways occurring within PSII and at the PSII-electrode interface, and includes the new mechanism of H_2O_2 photogeneration by PSII uncovered in this study.

We propose that the H_2O_2 photogeneration pathway identified may also exist in nature. The photo-generation of ROS by PSII, in particular H_2O_2, has been known to occur both *in vitro and in vivo*;44,45 but the source/mechanism of H_2O_2 generation has been contentious.45,46 Until now, antenna Chl *a* have only been associated with energy transfer, but the reduction of O_2 to form $O_2^{\bullet-}$ by Chl a^-/Chl a^* (in the antenna and RC complex) has the greatest thermodynamic driving force than any other potential sources. Chl a^* may be reduced by a nearby reductant such as a β-car or components within the thylakoid membrane when an electrode is not available.

Knowledge of the competing pathway will impact on photobioelectrodes incorporating photosystems, reaction centers and whole cells with respect to energy conversion efficiency and device stability. Conductive matrices or high surface area electrodes are often employed to improve loading or interfacial wiring within photoelectrodes. Additionally, electrode materials and electron mediators are often chosen based on their low reactivity for O_2 reduction to limit charge recombination and improve the open circuit voltage of biophotovoltaic cells. It is now apparent that ET to Chl *a* should also be minimized to limit side charge leakage pathways and H_2O_2 generation, which is detrimental to device stability.

Lastly, the advancement of PF-PEC as a chemical biology tool will heavily depend on improvements in the enzyme-electrode interface. In the future, advanced spectroscopic techniques, such as ultrafast laser spectroscopy, can be coupled to PF-PEC to provide a more holistic approach to characterize the kinetics and energetics of photo-active enzymes.

Online Methods

Source data

Experimental data that support the findings of this study are available at the University of Cambridge data repository (http://dx.doi.org/10.17863/CAM.747) or from the corresponding author.

Materials

All chemicals, including 2,6-dichloro-1,4-benzoquinone (DCBQ, 98%, Sigma Aldrich), 2-(N-morpholino)ethanesulfonic acid (MES, >98%, Alfa Aesar), $CaCl_2$ (>99%, Sigma Aldrich), $MgCl_2$ (98%, Fisher Scientific), KCl (99%, Alfa Aesar), glycerol (>99%, VWR Chemicals), KOH (>99%, Sigma Aldrich), betaine (98%, Fisher Scientific), NH_4OH (30%) solution (Fisher Scientific), H_2O_2 (30%) solution (Fisher Scientific), 3'-(3,4-dichlorophenyl)-1'1'-dimethylurea (DCMU, 98%, Alfa Aesar), spinach chlorophyll a (Sigma Aldrich), C_{60}-(N,N-dimethyl pyrrolidinium) idodide (>99% over all isomers, Solaris

Chem. Inc.), bovine liver catalase (Sigma Aldrich), bovine erythrocyte superoxide dismutase (Sigma Aldrich), glucose oxidase from *Aspergillus niger* (Sigma Aldrich), polystyrene beads (Polysciences, Inc.), ITO nanoparticles (Sigma Aldrich) and fluoride-dope tin oxide (FTO) coated glass (Sigma Aldrich) were purchased from commercial suppliers and used without further purification unless otherwise noted. Reagents for the analytical part of the work were of the highest available purity. *T. elongatus* PSII was kindly provided by Prof William A. Rutherford, from the Imperial College London.

Preparation of enzymes

Thermosynechococcus elongatus—BP-1 PSII core particles were isolated from a CP47 His-tagged mutant by Ni^{2+}-affinity chromatography based on previously reported methods,48 with minor alterations.6 The resultant PSII solution was determined to be ca. 2.4 mg Chl *a* mL^{-1} in concentration, with activity of ca. 3500 μmol O_2 mg (Chl *a*)$^{-1}$ h^{-1}.

Spinach PS II core particles were isolated as previously described with some modifications. 49 PSII membranes were diluted in a BTS400 buffer solution [20 mM BisTris (pH 6.5), $MgCl_2$ (20 mM), $CaCl_2$ (5 mM), $MgSO_4$ (10 mM) and sucrose (0.4 M)]. A 10% (w/v) β-dodecyl maltoside (β-DM) solution was made using the BTS400 buffer solution, which was added to the PSII membrane solution to give a final concentration of 1.25% (w/v) β-DM and 1.75 mg Chl *a* ml^{-1}. The suspension was gently stirred whilst incubated at room temperature for 20 min. Any non-solubilized material was removed by centrifugation for 20 min at 40 000 x g. The supernatant was transferred to a Q-Sepharose column (Pharmacia LKB, 1 g dry weight (mg Chl)$^{-1}$) that has been equilibrated with BTS400 with 0.03% β-DM to separate LHC II from the PS II core. The column was washed with BTS400 plus 0.03% β-DM until the elute became almost colorless and the ratio of absorption amplitude at 675/650 nm was larger than 3. The PSII core particles were eluted from the column by adding $MgSO_4$ (75 mM) to the BTS400 with 0.03% β-DM buffer. The PSII core dimers were purified from the monomers by gel filtration chromatography (Supplementary Figure 15), using a Superdex 200 HR 10/30 column (GE Healthcare) with BisTris (20 mM pH 6,5), $MgCl_2$ (10 mM), NaCl (20 mM), 1.5% Taurine and 0.03% β-DM as mobile phase, with a flow rate of 25 ml h^{-1}.50 A Shimadzu LC-10AT VP diode array detector was used for absorption amplitude detection.

The antenna CP43 was isolated as described previously with some modifications.51 The first step of the isolation and purification of the CP43 involved the preparation of PSII core complexes from spinach as described above. Briefly, these preparations were Tris-washed, solubilized with β-DM, and subjected to ion-exchange chromatography. The CP43 was found in the fraction that did not bind to the column. This fraction was mixed with 50 mM Tris-HCl (pH10) and 0.03% β-DM until the final pH was 7.8. This fraction was loaded into a Q-Sepharose column equilibrated with 50 mM Tris-HCl (pH 7.8) and 0.03% β-DM. After the elute (which contained mainly free Chl) became colourless, CP43 was eluted with the same buffer with 50 mM $MgSO_4$. The purity of CP43 was verified by fast protein liquid gel filtration chromatography (Supplementary Figure 16), using a Superdex 200 HR 10/30 column (GE Healthcare) with 20 mM BisTris (pH 6,5), 10mM $MgCl_2$, 20mM NaCl, 1.5% Taurine and 0.03% β-DM as mobile phase and a flow rate of 25 ml h^{-1}.50

The isolated RC complex used in this study is also known as the D_1-D_2-cyt b_{559} particle and was isolated according to a previous literature procedure,12 and the purity was also verified using the same method as for the CP43 (Supplementary Figure 17). It contains four Chl *a*, two pheophytin molecules, two peripheral Chl *a* molecules, two *β*-car and a cytochrome b_{559}. The plastoquinones, non-heme Fe and the Mn_4Ca cluster were all lost in the isolation process.

Stock solutions of *T. elongatus* PSII (2.4 mg Chl *a* mL^{-1}, 77 μM), spinach PSII (0.35 mg Chl *a* mL^{-1}, 11 μM), antenna CP43 (1.0 mg Chl *a* mL^{-1}) and RC complex (0.15 mg Chl *a* mL^{-1}) were stored in small aliquots in a liquid N_2 dewar, and a new aliquot was thawed in each day of experiments. One in three dilution of the stock *T. elongatus* PSII solution was made immediately before adsorption on the electrodes to give a final concentration of 25.6 μM. Stock solutions of Chl *a* (100 μg ml^{-1}) and *β*-car (400 μg ml^{-1}) were prepared in ethanol in the dark and used immediately.

Preparation of inverse opal mesoporous ITO electrodes

The hierarchically structured ITO electrodes were prepared from ITO nanoparticles (< 50 nm diameter) and polystyrene beads (750 nm diameter, 2.54% w/v suspension in water) according to a previously published procedure.6 In this study, the electrodes were prepared with an ITO film thickness of 12 μm, and contain macroporous inverse opal chambers and channels with diameters of 750 nm and 100 nm, respectively, to facilitate the penetration of the PSII and other macromolecules into the electrode structure (Supplementary Figure 2). The rough mesoporous sub-structure offers further enhancement in surface area and thus anchoring sites for the enzymes. Before use in the experiments, the ITO electrodes were cleaned by incubation in a solution mixture containing H_2O_2 (30%), H_2O, NH_4OH (30%) in a 1:5:1 v/v ratio, at 70 °C for 15 min. The electrodes were then rinsed with water, air dried for 1 hour at 180 °C, and allowed to cool to room temperature.

The surface morphology of the electrodes was analyzed by scanning electron microscopy (SEM; Philips XL30). Feature dimensions have been measured by built-in software. The elemental composition was verified using Powder X-ray diffraction (XRD) analysis was carried out using an X'Pert PRO X-ray diffractometer (PANalytical B.V.).

Adsorption of bio-films onto electrodes

The Chl *a* pigment content within each biological sample used in the study was quantified using the absorption amplitude at λ_{665} (ε = 79.95 (mg Chl *a*)$^{-1}$ mL cm^{-1})52 minus the background at λ_{710nm}. Unless otherwise stated, *T. elongatus* PSII (1 μL, 25.6 μM), spinach PSII (2 μL, 11 μM), antenna CP43 solution (2 μL, 1.0 mg Chl *a* mL^{-1}), RC complex solution (2 μL, 0.15 mg Chl *a* mL^{-1}), Chl *a* (2 μL,100 μg ml^{-1}) and *β*-car (2 μL, 400 μg ml^{-1}) were drop-cast onto cleaned ITO electrodes with a geometrical surface area of 0.25 cm^2 and left to stand for 15 min in a closed Petri dish in the dark before being used in photoelectrochemical experiments.

To estimate the degree of protein-film retention on the electrodes following experiments, the protein-film modified electrodes were incubated for 10 min in the MES electrolyte buffer solution in the dark (to avoid confounding photodegradation effects). The ITO film from

each electrode was then scraped into MeOH (250 μL) and centrifuged for 5 min at 10 000 rpm. The absorbance $\Delta\lambda_{(665\text{-}710nm)}$ of the supernatant was measured to determine the amount of Chl *a* content that was adsorbed on the electrode surface. The adsorbed Chl *a* concentration was then expressed as a percentage of the original amount that was drop-cast on the electrode. Electrodes modified with films of *T. elongatus*, antenna CP43 and the RC complex exhibited on average 85% retention (n = 3), whereas those adsorbed with spinach PSII and Chl *a* molecules exhibited on average 65% and 40% retention (n = 3), respectively. Similarly, the retention of *β*-car molecules was determined based on the absorption amplitude at λ_{450nm}; adsorbed *β*-car molecules exhibited on average 45% retention (n = 3).

In experiments where C_{60} was co-adsorbed with PSII or Chl *a*, a suspension of C_{60} in MES electrolyte buffer solution (50 mg mL^{-1}, 45 mM) was first prepared and sonicated for 30 min. This suspension was combined with the PSII (25.6 μM) or Chl *a* (0.45 mM) in a ratio of 1:1 v/v. A volume of 2 μL of the PSII/C_{60} mixture and 2 × 2 μL of the Chl *a*/C_{60} mixture was drop-cast onto cleaned ITO electrodes. The electrodes were left to stand for 15 min in a closed Petri dish in the dark before being used in photoelectrochemical experiments.

Electrochemical experiments

All electrochemical experiments were performed on Ivium Compactstat or PalmSens Emstat potentiostats, and the temperature was maintained at 25 °C by the water jacket around the photoelectrochemical cell and a thermostat. Electrochemistry was conducted using an inverse opal mesoporous ITO or a glassy carbon electrode as the working electrode, a platinum counter electrode, and an Ag/AgCl reference electrode unless stated otherwise. The MES buffer electrolyte solution employed in the experiments contained $CaCl_2$ (20 mM), $MgCl_2$ (15 mM), KCl (50 mM) and MES (40 mM) and glycerol (5%), and adjusted to pH 6.5. Stationary working electrodes were employed and the electrolyte solution was not stirred unless otherwise stated. To achieve anaerobic conditions, a stream of Ar was bubbled through the electrolyte solution for 15 min before introducing the working electrode inside the cell. The set-up was purged for an additional 15 min before the start of the experiment, the headspace was purged during the electrochemical experiment. Anaerobicity was also achieved by the addition of glucose (5 mM), glucose oxidase (0.1 mg mL^{-2}) and catalase (0.05 mg mL^{-2}) in a separate control experiment.53 Where O_2/N_2 purge mixtures were required, a mass flow controller (Brooks Instrument, GF series) was used to control the ratio of O_2:N_2 gases.

The light source (Kodak S-AV 2000) employed in the photoelectrochemical experiments was a halogen lamp collimated by a plano-convex lens and filtered by a bandpass filter (679 nm, full width at half maximum: 10.3 nm). The light intensity was adjusted to 5 mW cm^{-2}. The final volume of the electrolyte solution used was 4 mL. All redox potentials are quoted against the standard hydrogen electrode (SHE), with the potentials being calculated using the following correction factor: $E_{SHE} = E_{Ag/AgCl} + 0.209$ V.

In chronoamperometry scans, the experimental regimes were very similar in each case. Each potential was held for at least 60 s before being stepped up by 0.1 V, starting at 0 V vs SHE. This regime allowed the electrode to equilibrate for 20 s in the dark at each new potential before being irradiated with red-light (679 nm, 5 mW cm^{-2}) for 30 s, followed by light off

for 10 s. Variations to the potential step sizes and the number of steps were introduced according to the needs of the experiment. Where DCMU or DCBQ were needed, stock DCMU and DCBQ solutions (100 mM, DMSO) were prepared, and 40 μL was added to the electrolyte solution to give a final concentration of 1 μM. Dark current spikes caused by stepping the potential were removed in all figures for clarity. All experiments were replicated three times, and the most representative scans are shown.

Action spectra measurement

A 300 W Xenon lamp coupled to an MSH300 monochromator (LOT Quantum design) was used in the action spectra measurements. The light intensity measured as a function of wavelength (full width half maximum: 20 nm) with a photodetector (SEL033/F/QNDS1/W) and power meter (ILT1400).

Supplementary Material

Refer to Web version on PubMed Central for supplementary material.

Acknowledgements

This work was supported by the U.K. Engineering and Physical Sciences Research Council (EP/H00338X/2 to E. Reisner), the U.K. Biology and Biotechnological Sciences Research Council (BB/K010220/1 to E. Reisner), a Marie Curie International Incoming Fellowship (PIIF-GA-2012-328085 RPSII to J.J.Z.). N.P. was supported by the Winton Programme for the Physics of Sustainability. E. Romero. and R.v.G. were supported by the VU University Amsterdam, the Laserlab-Europe Consortium, the TOP grant (700.58.305) from the Foundation of Chemical Sciences part of NWO, the Advanced Investigator grant (267333, PHOTPROT) from the European Research Council, and the EU FP7 project PAPETS (GA 323901). R.v.G. gratefully acknowledges his `Academy Professor' grant from the Royal Netherlands Academy of Arts and Sciences. We would also like to thank Miss Katharina Brinkert and Prof A. William Rutherford for a sample of *T. elongatus* PSII, and H. v. Roon for preparation of the spinach PSII samples. Lastly, we thank Mr David W. Wakerley and Mr Timothy E. Rosser for valuable discussions.

References

1. Suga M, et al. Native structure of photosystem II at 1.95 Å resolution viewed by femtosecond X-ray pulses. Nature. 2015; 517:99–103. [PubMed: 25470056]
2. Nath K, et al. Towards a critical understanding of the photosystem II repair mechanism and its regulation during stress conditions. FEBS Lett. 2013; 587:3372–3381. [PubMed: 24056074]
3. Kruse O, Rupprecht J, Mussgnug JH, Dismukes GC, Hankamer B. Photosynthesis: a blueprint for solar energy capture and biohydrogen production technologies. Photochem Photobiol Sci. 2005; 4:957–970. [PubMed: 16307108]
4. Kato M, Zhang JZ, Paul N, Reisner E. Protein film photoelectrochemistry of the water oxidation enzyme photosystem II. Chem Soc Rev. 2014; 43:6485–6497. [PubMed: 24668258]
5. Badura A, Kothe T, Schuhmann W, Rogner M. Wiring photosynthetic enzymes to electrodes. Energy Environ Sci. 2011; 4:3263–3274.
6. Mersch D, et al. Wiring of photosystem II to hydrogenase for photoelectrochemical water splitting. J Am Chem Soc. 2015; 137:8541–8549. [PubMed: 26046591]
7. Kato M, Cardona T, Rutherford AW, Reisner E. Photoelectrochemical water oxidation with photosystem II integrated in a mesoporous indium-tin oxide electrode. J Am Chem Soc. 2012; 134:8332–8335. [PubMed: 22548478]
8. Lai Y-H, Kato M, Mersch D, Reisner E. Comparison of photoelectrochemical water oxidation activity of a synthetic photocatalyst system with photosystem II. Faraday Discuss. 2014; 176:199–211. [PubMed: 25434986]

9. Yehezkeli O, et al. Integrated photosystem II-based photo-bioelectrochemical cells. Nat Commun. 2012; 3 1741/1-7.
10. Romero E, van Stokkum IHM, Novoderezhkin VI, Dekker JP, van Grondelle R. Two different charge separation pathways in photosystem II. Biochemistry. 2010; 49:4300–4307. [PubMed: 20415453]
11. Romero E, et al. Mixed exciton-charge-transfer states in photosystem II: stark spectroscopy on site-directed mutants. Biophys J. 2012; 103:185–194. [PubMed: 22853895]
12. Romero E, et al. Quantum coherence in photosynthesis for efficient solar-energy conversion. Nat Phys. 2014; 10:676–682. [PubMed: 26870153]
13. Renger G, Renger T. Photosystem II: The machinery of photosynthetic water splitting. Photosynth Res. 2008; 98:53–80. [PubMed: 18830685]
14. Ananyev G, Dismukes GC. How fast can photosystem II split water? Kinetic performance at high and low frequencies. Photosynth Res. 2005; 84:355–365. [PubMed: 16049797]
15. Terasaki N, et al. Photocurrent generation properties of Histag-photosystem II immobilized on nanostructured gold electrode. Thin Solid Films. 2008; 516:2553–2557.
16. Kato M, Cardona T, Rutherford AW, Reisner E. Covalent immobilization of oriented photosystem II on a nanostructured electrode for solar water oxidation. J Am Chem Soc. 2013; 135:10610–10603. [PubMed: 23829513]
17. Badura A, et al. Photo-induced electron transfer between photosystem 2 via cross-linked redox hydrogels. Electroanalysis. 2008; 20:1043–1047.
18. Cai P, et al. Co-assembly of photosystem II/reduced graphene oxide multilayered biohybrid films for enhanced photocurrent. Nanoscale. 2015; 7:10908–10911. [PubMed: 26055965]
19. Umena Y, Kawakami K, Shen J-R, Kamiya N. Crystal structure of oxygen-evolving photosystem II at a resolution of 1.9 Å. Nature. 2011; 473:55–60. [PubMed: 21499260]
20. Barber J, Morris E, Büchel C. Revealing the structure of the photosystem II chlorophyll binding proteins, CP43 and CP47. Biochim Biophys Acta Bioenerg. 2000; 1459:239–247.
21. Tributsch H. Reaction of excited chlorophyll molecules at electrodes and in photosynthesis. Photochem Photobiol. 1972; 16:261–269.
22. Kay A, Humphry-Baker R, Graetzel M. Artificial Photosynthesis. 2. Investigations on the mechanism of photosensitization of nanocrystalline TiO2 solar cells by chlorophyll derivatives. J Phys Chem. 1994; 98:952–959.
23. Miyasaka T, Watanabe T, Fujishima A, Honda K. Photoelectrochemical study of chlorophyll a multilayers on tin oxide electrode. Photochem Photobiol. 1980; 32:217–222.
24. Barazzouk S, Kamat PV, Hotchandani S. Photoinduced electron transfer between chlorophyll a and gold nanoparticles. J Phys Chem B. 2005; 109:716–723. [PubMed: 16866432]
25. Seely GR. The energetics of electron-transfer reactions of chlorophyll and other compounds. Photochem Photobiol. 1978; 27:639–654.
26. Wakerley DW, Reisner E. Oxygen-tolerant proton reduction catalysis: much O2 about nothing? Energy Environ Sci. 2015; 8:2283–2295.
27. Nakato Y, Chiyoda T, Tsubomura H. Experimental determination of ionization potentials of organic amines, β-carotene and chlorophyll a. Bull Chem Soc Jpn. 1974; 47:3001–3005.
28. Huang Z, et al. Dye-controlled interfacial electron transfer for high-current indium tin oxide photocathodes. Angew Chem Int Ed. 2015; 54:6857–6861.
29. Krieger-Liszkay A. Singlet oxygen production in photosynthesis. J Exp Bot. 2005; 56:337–346.
30. Bielski BHJ, Cabelli DE, Arudi RL, Ross AB. Reactivity of perhydroxyl/superoxide radicals in aqueous solution. J Phys Chem. 1985; 14:1041–1100.
31. Adamiak W, Opallo M. Electrochemical redox processes of fullerene C60 and decamethylferrocene dissolved in cast 1,2-dichlorobenzene film in contact with aqueous electrolyte. J Electroanal Chem. 2010; 643:82–88.
32. El-Khouly ME, Araki Y, Fujitsuka M, Watanabe A, Ito O. Photoinduced electron transfer between chlorophylls (a/b) and fullerenes (C60/C70) studied by laser flash photolysis. Photochem Photobiol. 2001; 74:22–30. [PubMed: 11460533]

33. Yamakoshi Y, et al. Active Oxygen Species Generated from Photoexcited Fullerene (C60) as Potential Medicines: O-•2 versus 1O2. J Am Chem Soc. 2003; 125:12803–12809. [PubMed: 14558828]
34. Allakhverdiev SI, et al. Redox potentials of primary electron acceptor quinone molecule (QA)- and conserved energetics of photosystem II in cyanobacteria with chlorophyll a and chlorophyll d. Proc Natl Acad Sci U S A. 2011; 108:8054–8058. [PubMed: 21521792]
35. Kato Y, Nagao R, Noguchi T. Redox potential of the terminal quinone electron acceptor QB in photosystem II reveals the mechanism of electron transfer regulation. Proc Natl Acad Sci U S A. 2016; 113:620–625. [PubMed: 26715751]
36. Shibamoto T, et al. Species-dependence of the redox potential of the primary quinone electron acceptor QA in photosystem II verified by spectroelectrochemistry. FEBS Lett. 2010; 584:1526–1530. [PubMed: 20211622]
37. Léger C, Bertrand P. Direct electrochemistry of redox enzymes as a tool for mechanistic studies. Chemical Reviews. 2008; 108:2379–2438. [PubMed: 18620368]
38. Stevenson GP, et al. Theoretical analysis of the two-electron transfer reaction and experimental studies with surface-confined cytochrome c peroxidase using large-amplitude Fourier transformed AC voltammetry. Langmuir. 2012; 28:9864–9877. [PubMed: 22607123]
39. Johnson GN, Rutherford AW, Krieger A. A change in the midpoint potential of the quinone QA in Photosystem II associated with photoactivation of oxygen evolution. Biochim Biophys Acta Bioenerg. 1995; 1229:202–207.
40. Shibamoto T, Kato Y, Sugiura M, Watanabe T. Redox potential of the primary plastoquinone electron acceptor QA in photosystem II from Thermosynechococcus elongatus determined by spectroelectrochemistry. Biochemistry. 2009; 48:10682–10684. [PubMed: 19835366]
41. Alcantara K, Munge B, Pendon Z, Frank HA, Rusling JF. Thin film voltammetry of spinach photosystem II. proton-gated electron transfer involving the Mn4 cluster. J Am Chem Soc. 2006; 128:14930–14937. [PubMed: 17105304]
42. Satoh K, Oh-hashi M, Kashino Y, Koike H. Mechanism of electron flow through the QB site in photosystem II. 1. Kinetics of the reduction of electron acceptors at the QB and plastoquinone sites in photosystem II particles from the cyanobacterium Synechococcus vulcanus. Plant Cell Physiol. 1995; 36:597–605.
43. Kashino Y, Yamashita M, Okamoto Y, Koike H, Satoh K. Mechanisms of electron flow through the OB site in photosystem II. 3. Effects of the presence of membrane structure on the redox reactions at the QB site. Plant Cell Physiol. 1996; 37:976–982.
44. Pospisil P. Molecular mechanisms of production and scavenging of reactive oxygen species by photosystem II. Biochim Biophys Acta Bioenerg. 2012; 1817:218–231.
45. Pospisil P. Production of reactive oxygen species by photosystem II. Biochim Biophys Acta Bioenerg. 2009; 1787:1151–1160.
46. Vöpel T, et al. Simultaneous measurements of photocurrents and H2O2 evolution from solvent exposed photosystem 2 complexes. Biointerphases. 2016; 11:019001.
47. Ishikita H, Knapp E-W. Redox potentials of chlorophylls and β-carotene in the antenna complexes of photosystem II. J Am Chem Soc. 2005; 127:1963–1968. [PubMed: 15701031]
48. Sugiura M, Inoue Y. Highly purified thermo-stable oxygen-evolving photosystem II core complex from the thermophilic cyanobacterium Synechococcus elongatus having His-tagged CP43. Plant Cell Physiol. 1999; 40:1219–1231. [PubMed: 10682344]
49. Van Leeuwen PJ, Nieveen MC, Van de Meent EJ, Dekker JP, Van Gorkom HJ. Rapid and simple isolation of pure photosystem II core and reaction center particles from spinach. Photosynth Res. 1991; 28:149–153. [PubMed: 24414974]
50. Van Roon H, Van Breemen JFL, De Weerd FL, Dekker JP, Boekema EJ. Solubilization of green plant thylakoid membranes with n-dodecyl-α,D-maltoside. Implications for the structural organization of the photosystem II, photosystem I, ATP synthase and cytochrome b6f complexes. Photosynth Res. 2000; 64:155–166. [PubMed: 16228454]
51. Groot M-L, et al. Spectroscopic properties of the CP43 core antenna protein of photosystem II. Biophys J. 1999; 77:3328–3340. [PubMed: 10585955]

52. Porra RJ, Thompson WA, Kriedemann PE. Determination of accurate extinction coefficients and simultaneous equations for assaying chlorophylls a and b extracted with four different solvents: verification of the concentration of chlorophyll standards by atomic absorption spectroscopy. Biochim Biophys Acta Bioenerg. 1989; 975:384–394.

53. Merry SAP, et al. Modulation of quantum yield of primary radical pair formation in photosystem II by site-directed mutagenesis affecting radical cations and anions. Biochemistry. 1998; 37:17439–17447. [PubMed: 9860859]

Europe PMC Funders Author Manuscripts

Europe PMC Funders Author Manuscripts

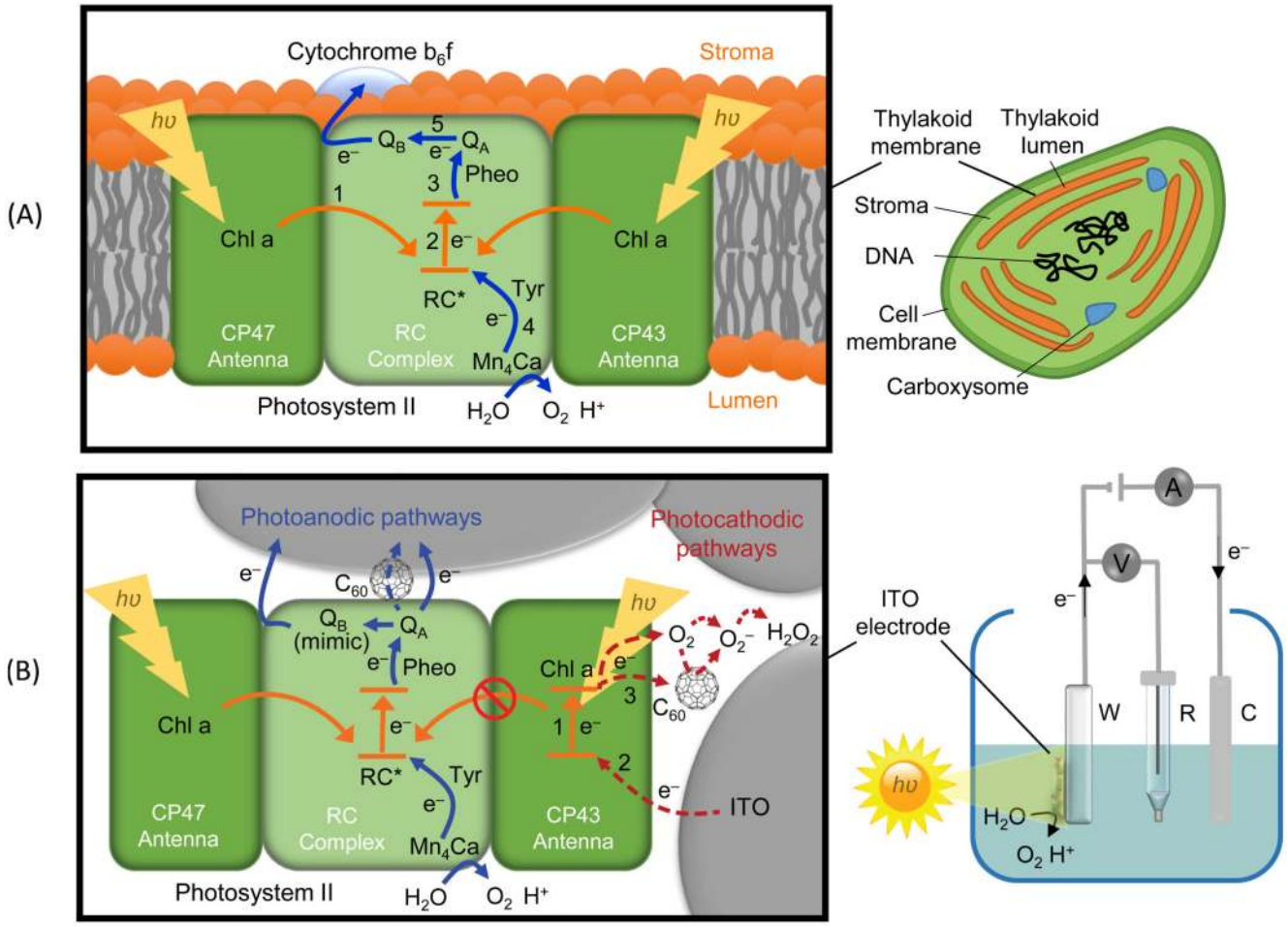

Figure 1. Schematic representation of the energy/charge transfer pathways within (A) PSII in the thylakoid membrane of a cyanobacterium; and (B) PSII adsorbed on a mesoporous indium-tin oxide (ITO) electrode connected to a photoelectrochemical cell.

The sequence of the water-oxidation pathway is given by the numbers in bold. The **orange** arrows represent energy transfer pathways resulting from light (*hυ*) absorption. The **blue** arrows represent electron transfer pathways taking place during oxygenic photosynthesis that give rise to the photoanodic currents detected by PF-PEC. The **red** arrows represent the competing O_2 reduction pathways that give rise to the photocathodic pathways detected by PF-PEC. Electron acceptors such as fullerenes (C_{60}) can enhance both the photoanodic and photocathodic pathways. The **solid arrows** represent known pathways including: energy transfer at the chlorophyll *a* (Chl *a*), charge generation/separation at the reaction center (RC), electron transfer via the pheophytin (Pheo), mediated Q_B/chemical mimic charge transfer,42,43 direct electron transfer from Q_A to the electrode,7 hole transfer via the tyrosin (Tyr) and water oxidation at the Mn_4Ca cluster. The **dashed arrows** represent new pathways identified using protein-film photoelectrochemistry under a three-electrode configuration comprising of a working (W), counter (C) and reference (R) electrode. Note that the depiction of the photocathodic pathway at the antenna CP43 subunit is arbitrary.

Europe PMC Funders Author Manuscripts

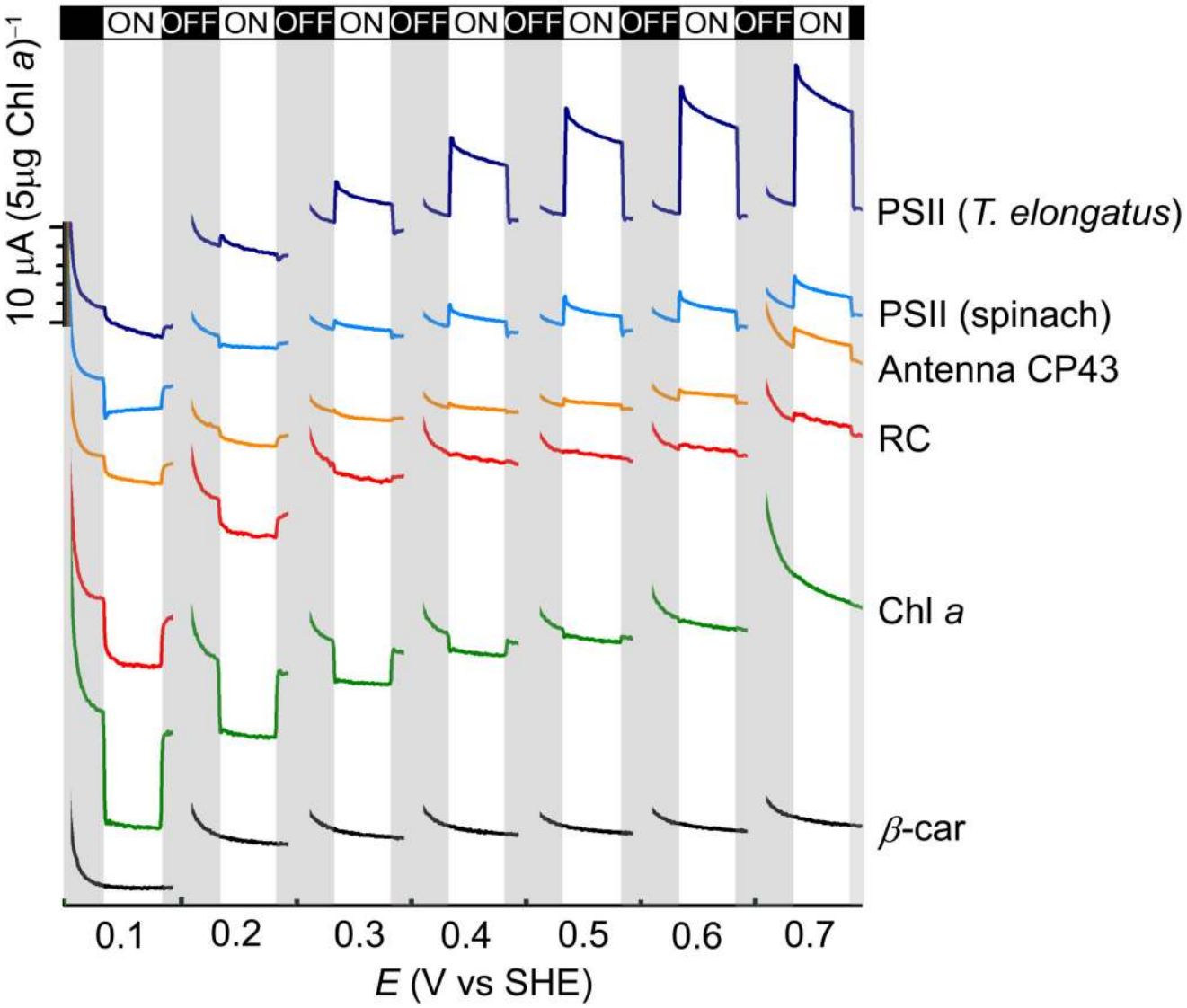

Figure 2. PSII photocathodic currents stem from protein-bound and isolated Chl *a* pigments.

Stepped chronoamperometry scans of PSII core complexes isolated from *T. elongatus* (**dark blue**) and spinach (**light blue**); and spinach CP43 antenna subunits (**orange**), spinach RC complexes with the Mn_4Ca cluster depleted (**red**), Chl *a* molecules (**green**), and *β*-carotene (*β*-car) molecules (**black**) adsorbed on hierarchically structured ITO electrodes. Potentials steps of 0.1 V were scanned in the anodic direction. All experiments were performed in a MES buffer electrolyte solution (pH 6.5) under aerobic conditions at 25 °C with chopped light illumination (679 nm, 5 mW cm^{-2}). Representative photo-responses are shown and the applied potentials are referenced against the standard hydrogen electrode (SHE); dark current spikes caused by the potential changes were removed for clarity. The photoresponses were normalized to the concentration of Chl *a* deposited on the electrode (5 μg Chl *a* cm^{-2} electrode surface area).

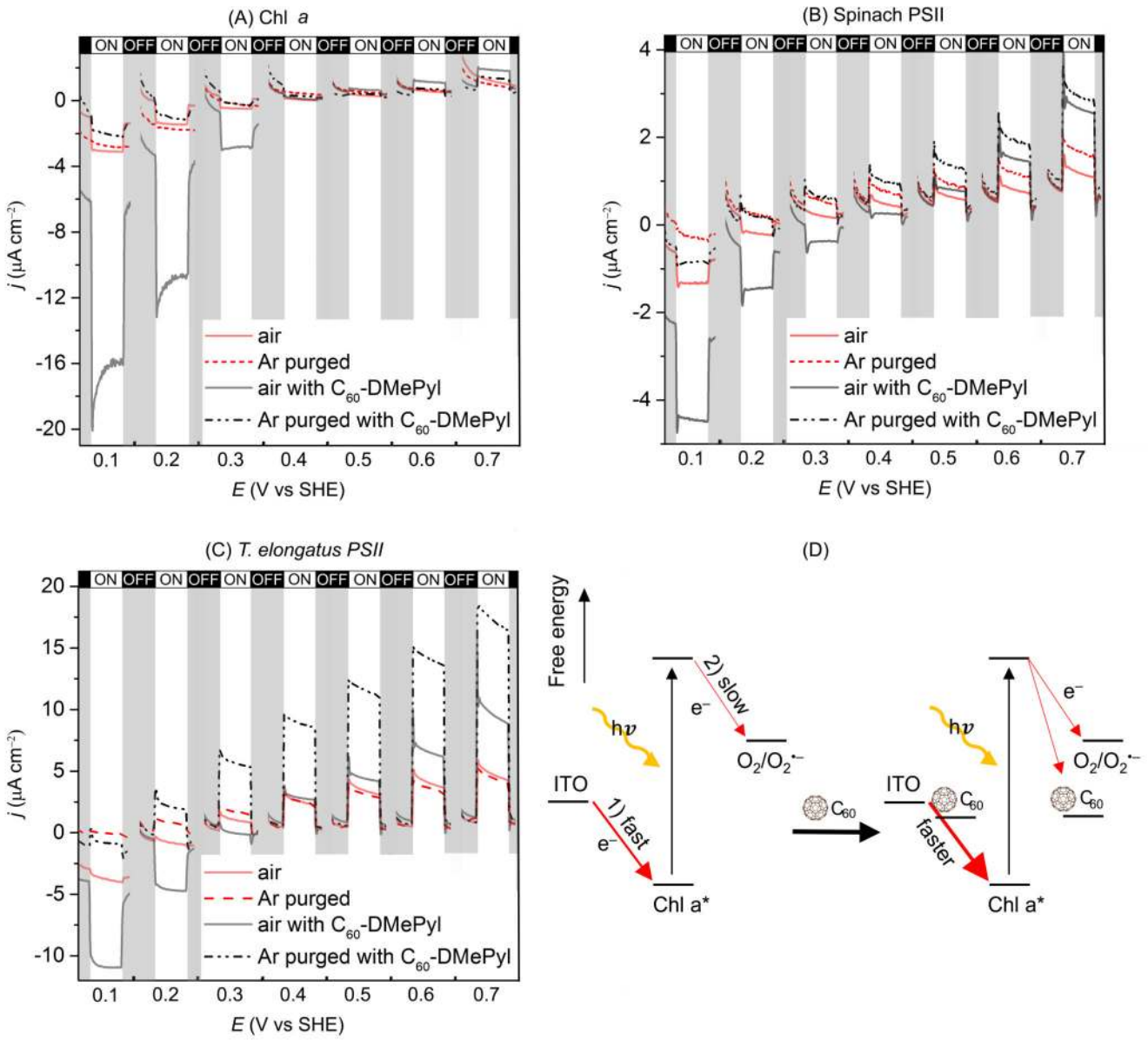

Figure 3. O_2 and the fullerene derivative, C60-DMePyI, are electron acceptors for photoexcited Chl *a*.

Photoresponse of **(A)** Chl *a*, **(B)** spinach PSII core complexes, and **(C)** *T. elongatus* PSII core complexes adsorbed on ITO electrodes in the presence (**black traces**) and absence (**red traces**) of a C_{60}-DMePyl matrix. Stepped chronoamperometry was performed under both aerobic (air, **solid traces**) and anaerobic (Ar purged, **dashed traces**) conditions in MES electrolyte buffer solution (pH 6.5) at 25°C with chopped red light illumination (679 nm, 5 mW cm^{-2}). Potentials steps of 0.1 V were scanned in the anodic direction and representative photoresponses are shown. **(D)** Proposed mechanisms of photocathodic current generation by Chl *a** in the presence of O_2, with enhanced photocathodic currents in the presence of a C_{60}-DMePyl matrix.

Europe PMC Funders Author Manuscripts

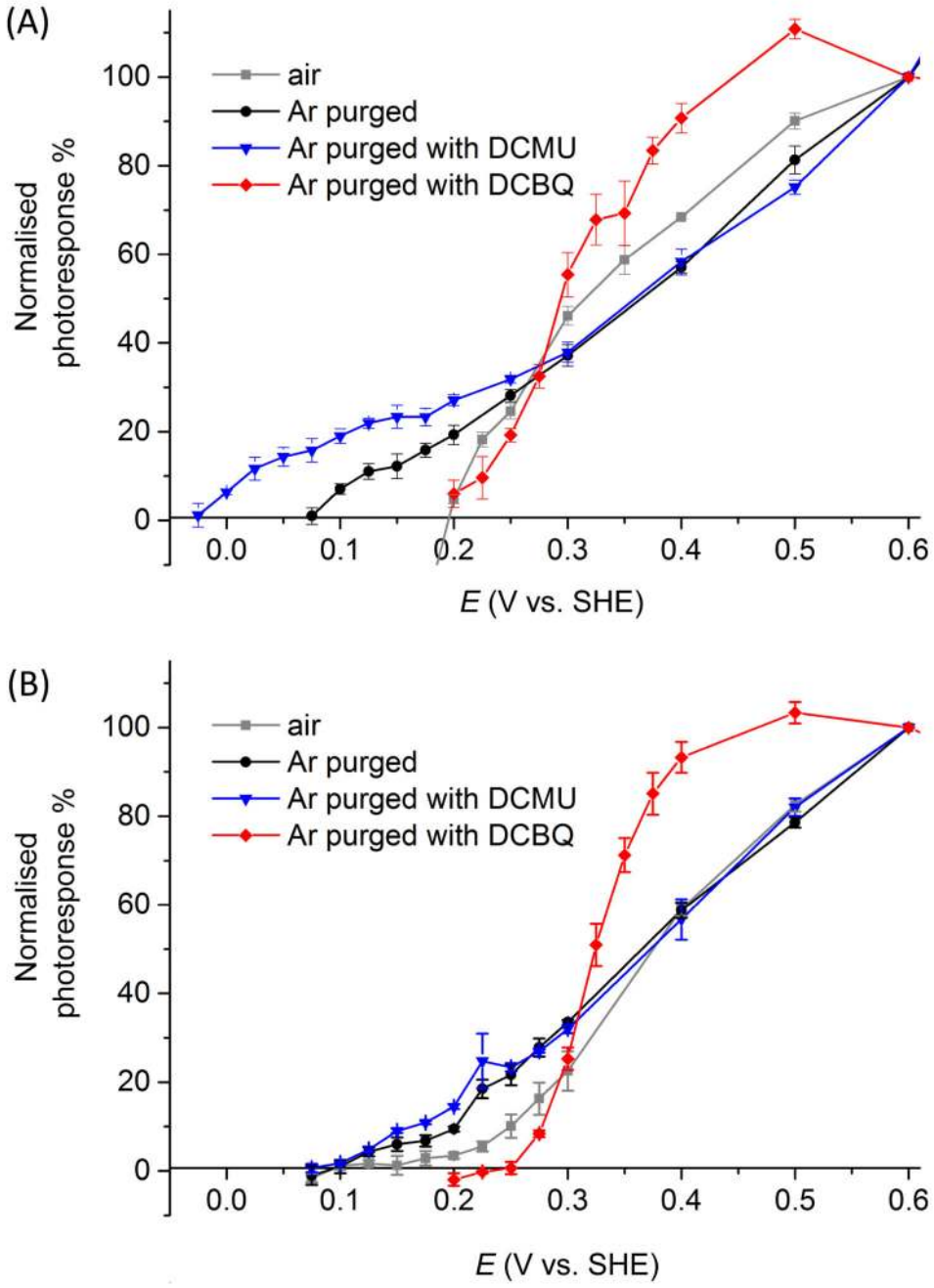

Figure 4. Onset potential determination of (A) spinach PSII and (B) *T. elongatus* PSII adsorbed on ITO electrodes.

Photoresponse plots from stepped chronoamperometry scans performed in the anodic direction. Experiments were conducted in aerobic (air, **grey trace**), anaerobic (argon (Ar) purged, **black trace**) conditions; and in the presence of the Q_B inhibitor, 3'-(3,4-dichlorophenyl)-1'1'-dimethylurea (DCMU, **blue trace**) and the Q_B mimic, 2,6-dichloro-1,4-benzoquinone (DCBQ, **red trace**). All experiments were conducted in MES electrolyte buffer solution (pH 6.5) at 25°C with light illumination (679 nm, 5 mW cm^{-2}),

and the photoresponses were normalized such that the photocurrent density at 0.6 V is equivalent to 100%. The error bars represent the standard error of the mean (n = 3).

Europe PMC Funders Author Manuscripts

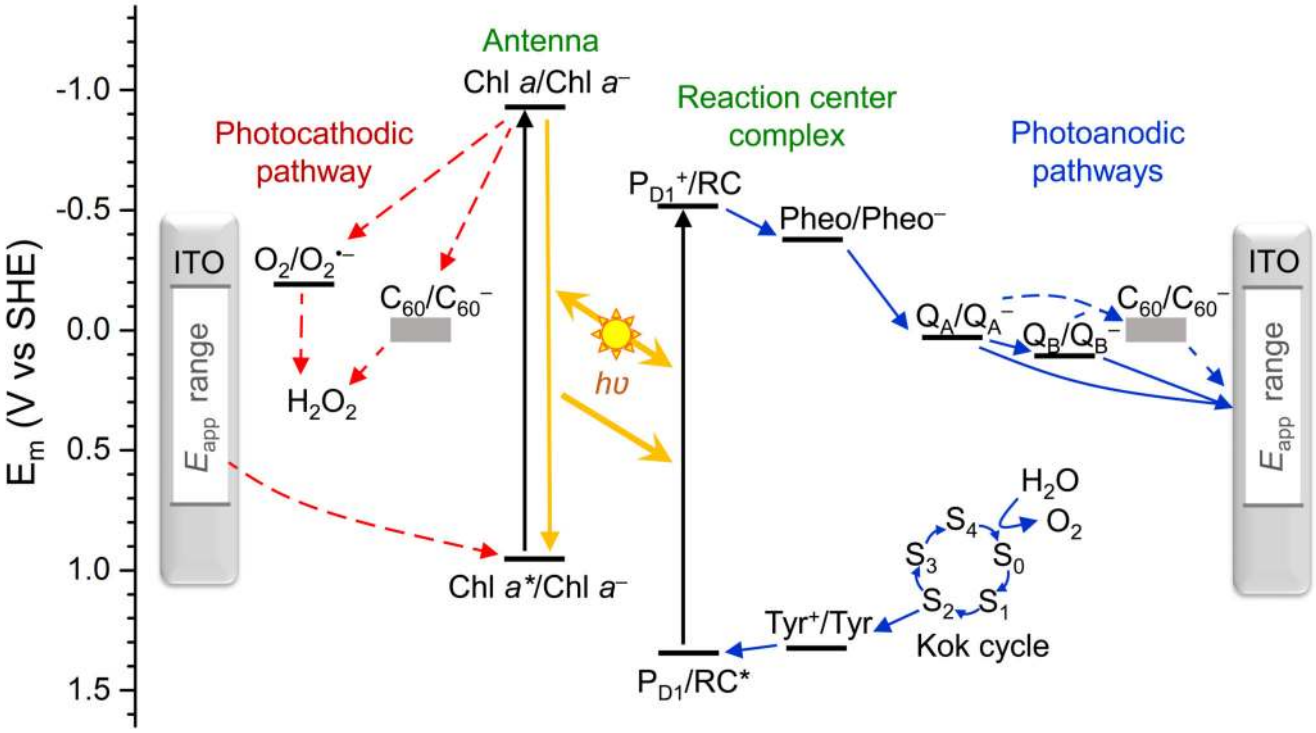

Figure 5. Summary of the photoanodic (blue) and photocathodic (red) charge transfer pathways within PSII and at the PSII-electrode interface.

The applied potential (E_{app}) range used in this study is shown. Energy levels of materials and cofactors are based on numbers reported within references.4,26,47 The P_{D1}/RC is also commonly referred to as the P680. **Grey** bars represent uncertain energy levels. The **dashed** arrows represent pathways and energy levels identified by this study.

Europe PMC Funders Author Manuscripts